EUROfusion

WPMAG-CPR(17) 18426

P Bruzzone et al.

A Prototype Conductor by React&Wind Method for the EUROfusion DEMO TF Coils

Preprint of Paper to be submitted for publication in Proceeding of 25th International Conference on Magnet Technology

This work has been carried out within the framework of the EUROfusion Consortium and has received funding from the Euratom research and training programme 2014-2018 under grant agreement No 633053. The views and opinions expressed herein do not necessarily reflect those of the European Commission.

A Prototype Conductor by React&Wind Method for the EUROfusion DEMO TF Coils

Pierluigi Bruzzone, Kamil Sedlak, Xabier Sarasola, Boris Stepanov, Davide Uglietti, Rainer Wesche, Luigi Muzzi, Antonio della Corte

***Abstract*— The React&Wind (RW) method for the large Nb_3Sn magnets of the EUROfusion DEMO device was proposed since 2013 by the Swiss Plasma Center. A first short length prototype conductor for the toroidal field (TF) coils, named RW1, was tested in the EDIPO test facility in 2015-2016 up to 82 kA at 13 T, with an effective strain matching the expected thermal strain of ≈-0.30%. After the baseline of the DEMO device was updated in 2015, the new requirements led to an updated conductor design, for 63 kA at 12.2 T. The manufacturing experience of the first prototype is exploited in a second short length prototype conductor, named RW2, assembled and tested in 2017: the conductor aspect ratio is reduced and the segregated copper wires are replaced by a solid block of mixed matrix stabilizer. Although designed for the TF coils, with DC operation, the moderate AC loss of the flat cable makes the RW2 a good candidate also for the Central Solenoid (CS) conductor.**

The Nb_3Sn strand for RW2 is supplied by WST (PRC) and the flat cable is made at TRATOS (I). The rationale of the design, the conductor manufacture, the sample assembly and the test results in SULTAN are reported.

***Index Terms*—React & Wind, Prototype Test, Conductor design, Fusion Magnets, Force Flow Conductors, .**

I. Introduction

The conceptual studies for a tokamak demonstration fusion power plant (DEMO) started in 2012 and are included since 2014 in the program of the EUROfusion consortium [1]. The engineering design phase of DEMO is expected to start ≈ 2027. The Swiss Plasma Center (SPC), ENEA and many other European laboratories participate to the conceptual studies of the magnet system with design and R&D tasks monitored by EUROfusion [2].

The Toroidal Field (TF) magnets of ITER were designed in 1995 and will be fully validated/ commissioned 30 years later. The efforts of SPC, ENEA and other European labs address design and technology issues, which emerge during the ITER coil manufacture and explore options to improve the cost, effectiveness, reliability and lifetime.

In the React&Wind (RW) method for Nb_3Sn magnets, the conductor is wound in its final form after the heat treatment, which is carried out without steel conduit and electrical insulation. The RW method is suitable for large coils with large bending radii. It offers remarkable advantages, e.g. low thermal strain for Nb_3Sn, tolerance to dimensional hysteresis upon heat treatment, simplified winding/insulating (same as NbTi coils). The RW method was used in several fusion magnets [3], e.g. T-15, TRIAM, MFTF, DPC-EX and the SULTAN coils.

SPC and ENEA developed and tested a TF prototype conductor for the DEMO baseline 2014, named RW1 [4-6]. The new RW2 prototype, whose manufacture and test are discussed here, is designed for the baseline 2015 [6] and is relevant also for the newly issued 2017 DEMO baseline [7].

II. From RW1 to RW2 Prototype Conductors

The layout of RW1 and RW2 prototypes is listed in Table I and Fig. 1. Both conductors are based on a superconducting flat cable, to keep the Nb_3Sn strand close to the neutral bending axis, and two steel shells, assembled by longitudinal laser welding. From RW1 to RW2, the aspect ratio is reduced from 2.9 to 1.9 and the inner corner of the conduit is increased from 3 mm to 8 mm as a feedback from the result of the stress analysis [8]. For the segregated copper the layer of thick copper wires in RW1 is replaced by two solid profiles of Cu/CuNi mixed matrix stabilizer in RW2. The thickness of the flat cable is reduced from 12.3 mm in RW1 to 11.0 mm in RW2 for a higher bending tolerance.

TABLE I
Layout of the RW1 and RW2 Prototype Conductors

	RW1	RW2
Operating Current, kA	82.4	63.3
Peak Operating Field, T	13.5	12.23
Width x height, mm x mm	100 x 34	61.5 x 32.1
Strand Diameter, mm	1.5	1.2
Cable Layout	(1 Cu +6+12) x 17	(1 Cu +6+12) x 13
Cable pitches, mm	+90 +185 / -595	+105 / +390
SC cable size, mm x mm	62.0 x 12.3	35 x 11
Void fraction in cable	≈ 27%	≈ 23%
J_{copper}, A/mm^2	119	90
$J_{non\text{-}copper}$, A/mm^2	305	478
Central strip in flat cable	none	Steel, 25mm x 0.2mm
Steel cross section, mm^2	2060	893.5
Conduit inner radius, mm	3	8

This work has been carried out within the framework of the EUROfusion Consortium and has received funding from the Euratom research and training programme 2014-2018 under grant agreement No 633053. The views and opinions expressed herein do not necessarily reflect those of the European Commission.

Pierluigi Bruzzone, Kamil Sedlak, Xabier Sarasola, Boris Stepanov, Davide Uglietti and Rainer Wesche are with EPFL-Swiss plasma Center, 5232 - Villigen PSI, Switzerland (e-mail: pierluigi.bruzzone@psi.ch, kamil.sedlak@psi.ch, xabier.sarasola@psi.ch, boris.stepanov@psi.ch, davide.uglietti@psi.ch, rainer.wesche@psi.ch).

Luigi Muzzi and Antonio della Corte are with ENEA, 00044 Frascati, Italy (e-mail: luigi.muzzi@enea.it, antonio.dellacorte@enea.it).

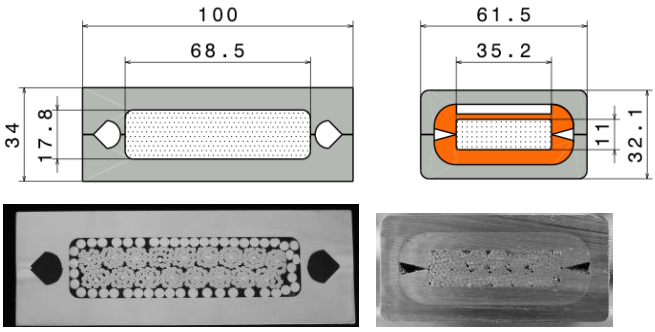

Fig. 1. Cross sections of RW1 (left) and RW2 (right). The RW2 picture of the SULTAN sample has brass profiles instead of mixed matrix stabilizer.

III. RW2 Manufacture and Sample Assembly

A. Nb_3Sn Strand

The cr plated Nb_3Sn strands for RW2 are kindly offered by WST. The J_c performance measured on pre-production sections, $J_c \approx 1130$ A/mm^2 @ 12 T / 4.2 K [6] suggested reducing the number of sub-cables in RW2 from 14 to 13 to avoid overdesign. However, the RW2 witness strand samples (barrels) included in the heat treatment of the cable gave a slightly lower performance, $J_c \approx 1078$ A/mm^2 @ 12 T / 4.2 K, which is only 1.07 times higher than the witness strands of RW1. The RW2 strand is also tested at variable temperature and strain at the University of Geneva [9].

The strand results are gathered in Fig. 2. The solid lines are fitting of the experimental results from [9] at 11, 13 and 15 T. The dashed line is the scaling law of RW1 [10] multiplied by 1.07. The dotted lines are the RW2 witness strands on barrel results at 11, 13 and 15 T, suggesting a large, about -0.29% "strain on barrel", when correlated with the results from [9], or a smaller, -0.15% "strain on barrel", when correlated with the results from [10] multiplied by a 1.07 factor.

B. Cable work

The two-stage flat cable was manufactured by ENEA at TRATOS (I). A bare copper wire is used as a core for the 1+6+12 first stage, stranded in one go with 105 mm twist pitch. The flat cable with central steel strip slightly exceeds

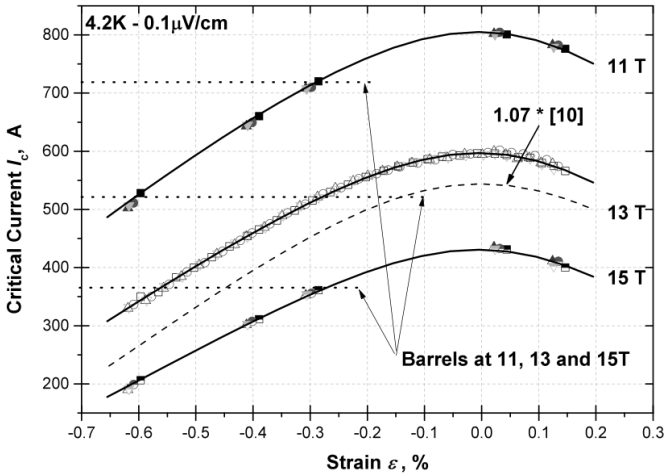

Fig. 2. Strand test results: $I_c(\varepsilon)$ from [9] together with the witness strand results on barrel (dotted line) and the scaling law from [10].

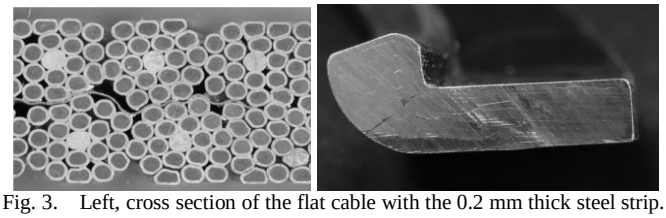

Fig. 3. Left, cross section of the flat cable with the 0.2 mm thick steel strip. Right, cross section of the mixed matrix trial (half profile).

the design size (35 mm x 11 mm instead of 35 mm x 10.5 mm) due to the spring back after the compaction rolls. The estimated void fraction is ≈23% compared to the design target of 20%. The steel strip deforms satisfactorily during the cable compaction, see Fig. 3 left. The total production length of the Nb_3Sn flat cable is 20.1 m.

C. Segregated Stabilizer

The manufacture of the mixed matrix stabilizer by extrusion in a CuNi10 can of a number of Ni plated Cu rods is delayed. A "half size" stabilizer is obtained by swaging and rolling small assemblies with ø = 30 mm, see Fig. 3 right. Extruded, drawn and rolled "full size" profiles are being completed in late 2017. The RW2 conductor with mixed matrix stabilizer will be tested in the end of 2017. As a temporary solution, for the RW2 conductor discussed here, the mixed matrix stabilizer is replaced by a brass profile, see Fig. 1.

D. Conduit and Welding

The longitudinal laser welding of the 316L conduit is carried out at Montansthal (CH). The small amount of the conduit sections is machined. An inquiry for hot rolled and cold drawn 316L profiles suggests a price of 5 €/kg for 5 t minimum amount.

So far, three heat treated cable sections, each 3.5 m long, have been encased in the steel conduit by laser welding, two sections are assembled with brass profiles and one (not yet tested) with mixed matrix half profiles.

E. Sample Assembly

The two RW2 sections with brass profiles are assembled into a SULTAN sample with termination and instrumentation as in the earlier RW1 sample [5]. After the first test campaign, the right section of the sample is cut and re-assembled with a joint [11]. The left section is bent at R = 8.3 m to reproduce the winding strain of the RW method, see Fig. 4, and straightened for test in the second campaign.

IV. Test Results and Discussion

The results reported below are from the first test campaign (DC performance, AC loss, warm-up/ cool-down, cyclic loading) and the second test campaign with the L section bent and straightened.

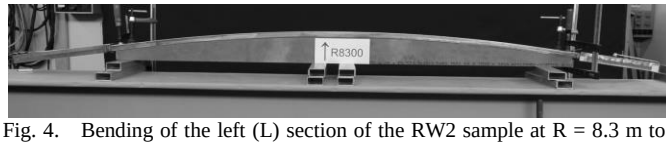

Fig. 4. Bending of the left (L) section of the RW2 sample at R = 8.3 m to demonstrate the reversibility of the RW winding process.

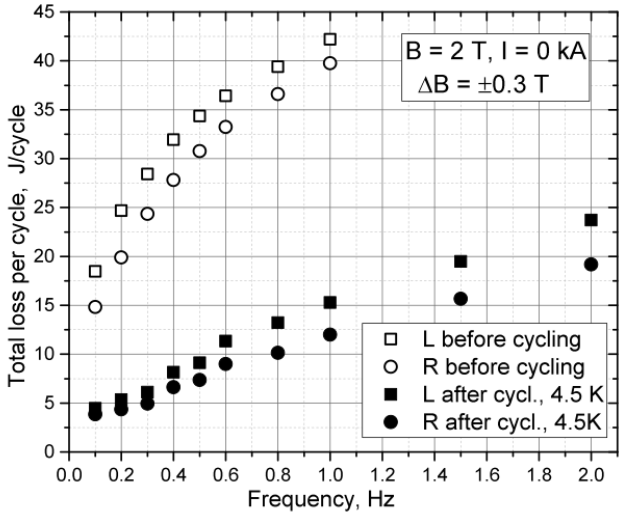

Fig. 5. Loss curve before and after cyclic loading.

A. AC loss

The results for sinusoidal field perpendicular to the broad side of the flat cable are shown in Fig. 5. As in most Nb_3Sn cable-in-conduit, the AC loss substantially decreases upon cyclic loading due to the disengagement of the low inter-strand contact resistance points. In a real R&W coil, the contact disengagement will happen during the handling, i.e. the results "before cyclic loading" have no technical relevance. It is not clear why the L section has systematically higher loss than the R section.

The loss in Fig. 5 accounts for hysteresis and coupling loss in the flat cable as well as eddy currents loss in the brass. The AC loss runs are repeated at 19 K operating temperature to single out the contribution of the eddy current loss. In Fig. 6 the average loss of R and L sections are compared at 4.5 K and 19 K operating temperature. The hysteresis loss contribution obviously disappears at 19 K. The time constant of brass, $n\tau_{\perp}^{brass} \approx 12\,ms$, is obtained by normalizing the 19 K loss to the brass volume. The coupling loss constant of the flat cable is obtained by normalizing to the flat cable volume the slope of the difference of the two curves in Fig. 6,

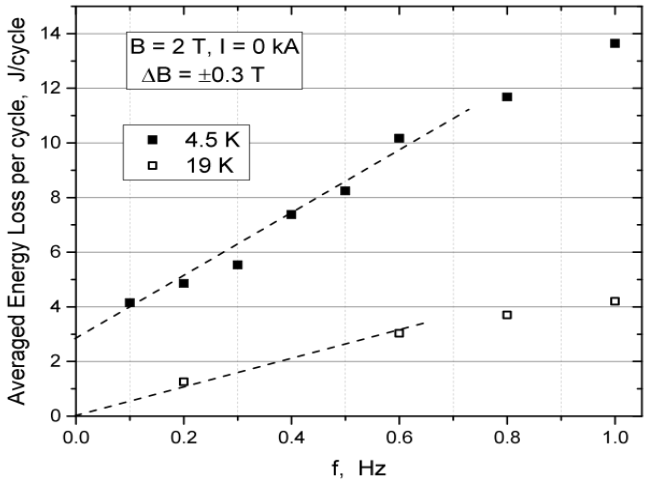

Fig. 6. AC loss curve at 4.5 K and 19 K operating temperature (average of L and R sections). At 19 K, the hysteresis and coupling currents loss vanish and only the eddy currents loss in the brass profiles remains.

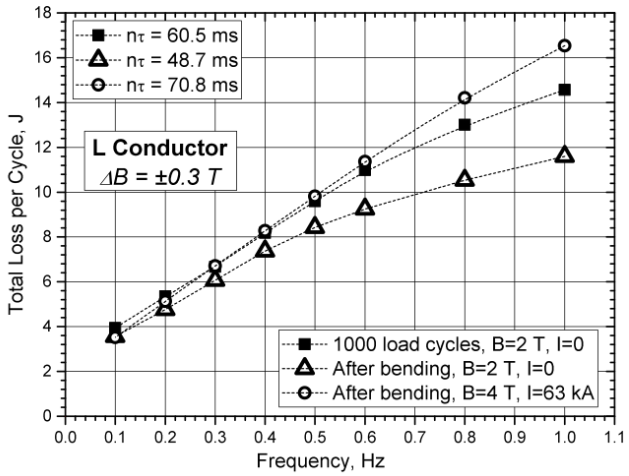

Fig. 7. AC loss and loss constant for L conductor.

$n\tau_{\perp}^{flat\,cable} = 50 \pm 10\,ms.$

From [12, 13] the coupling loss constant for field parallel to the broad side of the flat cable is estimated $n\tau_{\parallel}^{flat\,cable} < 10\,ms$.

The L sections has been tested for AC loss, with and without transport current, in the second campaign, after bending and straighteneing. The results are gathered in Fig. 7. The initial slope of the curve (the nτ value) slightly decreases upon bending straightening. The nτ increase with transport current due to the transverse compression is modest. The nτ in Fig. 7 is estimated by subtracting the eddy currents loss and normalizing to the cable (strand) volume.

B. DC Test Results

The DC test includes I_c and T_{cs} runs before and after 1100 load cycles and two warm-up/cool-down (wucd). The nominal operating point of 63.3 kA / 12.23 T cannot be achieved in the SULTAN test facility. To reproduce the correct B·I transverse load, the cyclic loading is applied at 70 kA and 10.9 T background field.

The baseline of the V(T) trace for the T_{cs} runs is not perfectly zero. A voltage offset ranging from 1.4 μV to 0.7 μV at 63 kA is observed and corrected in post-processing according to the procedure in [14]. The evolution of the T_{cs}

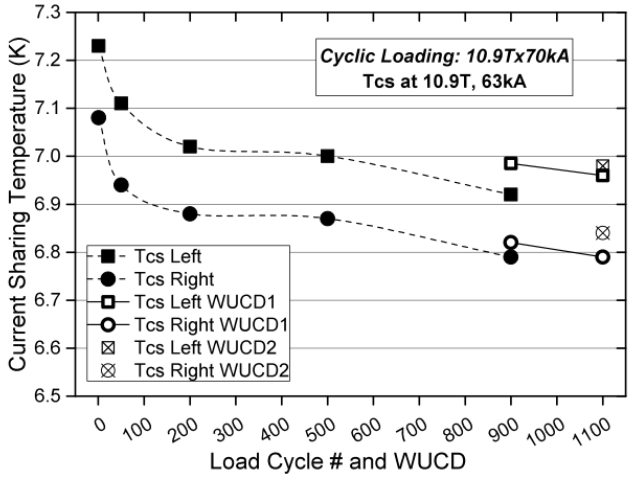

Fig. 8. Evolution of the T_{cs} performance upon cyclic loading and wucd.

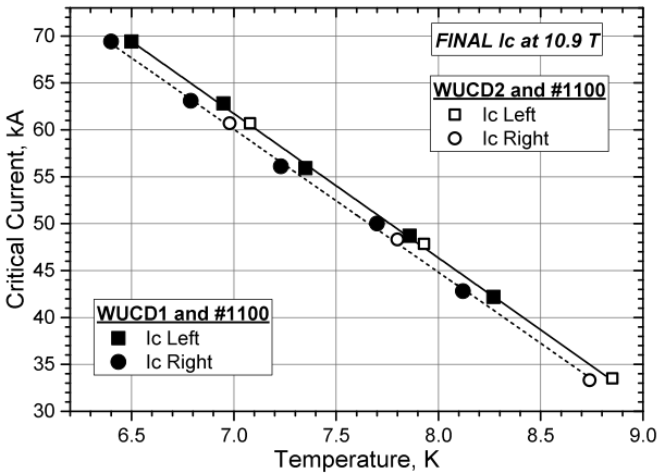

Fig. 9. I_c results at 10.9 T background field.

results at 10.9 T background field is summarized in Fig. 8. An unexpected performance drop by ≈ 0.25 K is observed upon cyclic loading, only marginally recovering upon wucd. The L section has better performance than R (≈ +0.15 K). The index of the T_{cs} transition remains constant over cyclic loading and wucd, suggesting that the degradation is related to a shift of the strain distribution rather than to filament breakage.

The $I_c(T)$ results after cyclic loading are gathered in Fig. 9. The n-index remains constant, ≈ 18, over the whole test campaign. The n-index of the free standing strands at comparable critical current (200-270 A/strand) is extrapolated to ≈18-20.

The T_{cs} at 63 kA is measured as a function of the background field for a reliable extrapolation to the nominal operating point, see Fig. 10. The B_{eff} = 12.23 T corresponds to a background field of 11.6 T, suggesting T_{cs} = 6.43 K and 6.26 K at the nominal operating point for L and R respectively.

C. Effective strain assessment

The "effective strain", ε_{eff}, is the parameter to be used in the strand scaling law to fit the conductor performance. For RW1, using the scaling law in [10], ε_{effRW1} = -0.28% / -0.35%. For a consistent approach with RW2, the 1.07 multiplier is applied to the scaling law in [10]. To match the RW2 results an effective strain of -0.35% (initial performance, left section) and -0.40% (final performance, left section) must be applied. The observed degradation in Fig. 8 corresponds to a change of ε_{eff} by 0.05%. The effective strain would be slightly larger retaining the scaling law from the results of [9], see Fig. 2 solid lines.

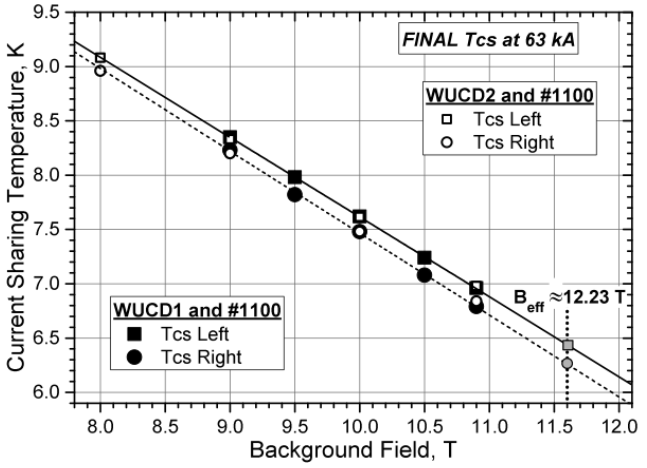

Fig. 10. T_{cs} vs. background field with extrapolation to the nominal operating point of B_{eff} = 12.23 T.

V. Outlook

To complete the development and characterization of the RW2 prototype conductor, the AC loss will be measured, at 4.5 K and 19 K, with AC field parallel to the broad side of the cable. Two more assembly will be done and tested with the mixed matrix stabilizer, "half profiles" and "full profiles".

VI. Conclusion

The manufacture of the short length prototype conductor according to the RW2 layout was satisfactory completed in Spring 2017, except for the mixed matrix stabilizer, for which the full test is scheduled in late 2017.

Despite the reduction of the cable cross section by 7% (13 instead of 14 sub-cables), the DC performance fulfils the design requirement, with T_{cs} ≈ 6.5 K at I_{op} = 63 kA and B_{eff} =12.23 T. An unexpected degradation by ≈ 0.25 K is observed upon cyclic loading. The index of superconducting transition does not decrease from the initial n = 18 despite the T_{cs} performance loss, suggesting a shift in the strain distribution rather than a filament breakage as a reason for the performance loss. The effective strain is ≈ -0.40 %, compared to ≈ -0.30% in the former prototype, RW1. The reason for the reduced effective strain is not clear so far.

The low AC loss results of the RW2 sample, nτ ≈ 50 ms for the strand volume, suggest a possible use of the same layout also for a CS conductor.

Acknowledgment

The authors are indebted with WST for the Nb_3Sn strand, with TRATOS for the cabling work and with Carmine Senatore for the $I_c(B, T, \varepsilon)$ test on the strand samples. The technical support of Paul Scherrer Institute, PSI, is acknowledged.

References

[1] http://www.eurofusion.org
[2] V. Corato et al., "EU Progress in Superconductor Technology Development for DEMO Magnets," presented at the ISFNT-13 Conf., Kyoto 2017.
[3] P. Bruzzone, "Superconducting Magnets for Fusion Reactors" and "Forced Flow Conductor Manufacturing", in *Engineering Superconductivity*, Lee PJ, editor, Wiley-Interscience, 2001.
[4] P. Bruzzone, K. Sedlak, B. Stepanov, "High current Superconductors for DEMO", *Fusion Engineering and Design* 88, 9-10, 1564-1568 (2013).
[5] P. Bruzzone et al., "Design, Manufacture and Test of a 82 kA React&Wind TF Conductor for DEMO," *IEEE Trans. Appl. Supercond.*, vol. 26, no. 4, 2016, Art. no. 4801805.
[6] K. Sedlak et al., "Design and R&D for the DEMO Toroidal Field Coils Based on Nb_3Sn React and Wind Method," *IEEE Trans. Appl. Supercond.*, vol. 27, no. 4, 2017, Art. no. 4800105.

[7] June-2017 DEMO Reference Configuration model, https://idm.euro-fusion.org/?uid=2N4EZW.
[8] A. Panin, "Structural issues for the 2015 TFC mechanical layout", https://idm.euro-fusion.org/?uid=2MPD7S.
[9] C. Senatore, private communication July 2017.
[10] A. Nijhuis, "TF conductor samples strand thermo mechanical critical performances tests", [Online]. Available: https://idm.euro-fusion.org/?uid=2M5SMM.
[11] B. Stepanov and P. Bruzzone, "Inter-layer Joint for the TF Coils of DEMO - Design and R&D," *IEEE Trans Appl. Supercond.*, to be published.
[12] P. Bruzzone, "AC losses in high current superconductors for nuclear fusion magnets," PhD Thesis ETH 8224, 1987.
[13] F. Cau and P. Bruzzone, "Dependence of the ac loss on the aspect ratio in a cable in conduit conductor," *Supercond. Sci. Technol*. 23 045011 2010.
[14] P. Bruzzone et al., "Methods, Accuracy and Reliability of ITER Conductor Tests in SULTAN," *IEEE Trans. Appl. Supercond.*, vol. 19, p 1508, 2009.

TABLE I
UNITS FOR MAGNETIC PROPERTIES (SHORT TITLE HERE IN SMALL CAPS)

Symbol	Quantity	Conversion from Gaussian and CGS EMU to SI [a]
Φ	magnetic flux	1 Mx $\rightarrow 10^{-8}$ Wb = 10^{-8} V·s
B	magnetic flux density, magnetic induction	1 G $\rightarrow 10^{-4}$ T = 10^{-4} Wb/m^2
H	magnetic field strength	1 Oe $\rightarrow 10^3/(4\pi)$ A/m
m	magnetic moment	1 erg/G = 1 emu $\rightarrow 10^{-3}$ A·m^2 = 10^{-3} J/T
M	magnetization	1 erg/(G·cm^3) = 1 emu/cm^3 $\rightarrow 10^3$ A/m
$4\pi M$	magnetization	1 G $\rightarrow 10^3/(4\pi)$ A/m
σ	specific magnetization	1 erg/(G·g) = 1 emu/g $\rightarrow$ 1 A·m^2/kg
j	magnetic dipole moment	1 erg/G = 1 emu $\rightarrow 4\pi \times 10^{-10}$ Wb·m
J	magnetic polarization	1 erg/(G·cm^3) = 1 emu/cm^3 $\rightarrow 4\pi \times 10^{-4}$ T
χ, κ	susceptibility	$1 \rightarrow 4\pi$
χ_ρ	mass susceptibility	1 cm^3/g $\rightarrow 4\pi \times 10^{-3}$ m^3/kg
μ	permeability	$1 \rightarrow 4\pi \times 10^{-7}$ H/m = $4\pi \times 10^{-7}$ Wb/(A·m)
μ_r	relative permeability	$\mu \rightarrow \mu_r$
w, W	energy density	1 erg/cm^3 $\rightarrow 10^{-1}$ J/m^3
N, D	demagnetizing factor	$1 \rightarrow 1/(4\pi)$

No vertical lines in table. Statements that serve as captions for the entire table do not need footnote letters. A longer description of the table would go here.

[a]Gaussian units are the same as cgs emu for magnetostatics; Mx = maxwell, G = gauss, Oe = oersted; Wb = weber, V = volt, s = second, T = tesla, m = meter, A = ampere, J = joule, kg = kilogram, H = henry.

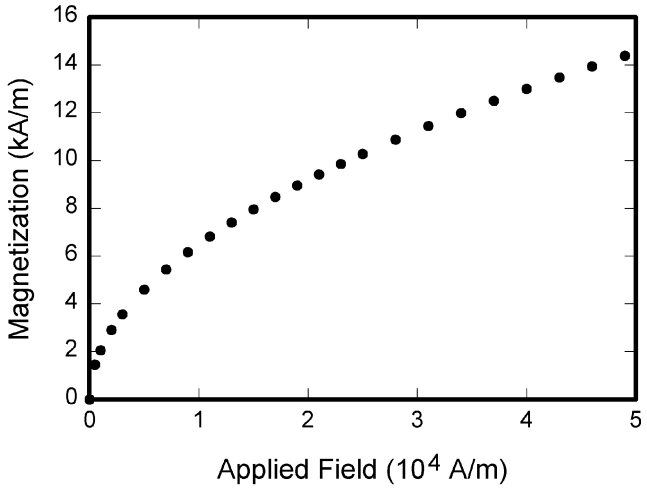

Fig. 2. Magnetization as a function of applied field. It is good practice to explain the significance of the figure in the caption. Note that "Fig." is abbreviated, and note that there is an em space after the number and period. This figure has been positioned according to Option 2 for manuscript preparation.